Cyclic stress fields ahead of tension fatigue cracks in amorphous polymers

L. Pruitt
Department of Mechanical Engineering, University of California, Berkeley, CA 94720, USA

and S. Suresh*
Department of Materials Science and Engineering, MIT, Room 13-5056, Cambridge, MA 02139, USA
(Received 1 December 1993)

Cyclic near-tip stress fields which evolve ahead of fatigue cracks are known to have a pronounced effect on the fracture response of materials. This region of reversed damage is responsible for the initiation of fatigue cracks from stress concentrations under fully compressive cyclic loads, crack growth retardation following tensile overloads, and transient crack growth response under spectrum fatigue loading. By recourse to photoelasticity and laser interferometry, we provide direct and *in situ* measurements of cyclic near-tip stresses ahead of notches and fatigue cracks in amorphous polymers subjected to cyclic tension loading. The near-tip stresses are quantified during both the loading and unloading phases of the fatigue cycle, as well as during various stages of crack advance, in an attempt to establish a link between the evolution of near-tip stress fields and the advance of the fatigue crack. In addition, transmission electron microscopy analyses of the near-tip region have been performed to characterize cyclic deformation mechanisms.

(Keywords: near-tip stress fields; cyclic damage; fatigue crack propagation)

INTRODUCTION

When a fatigue crack in an engineering material is subjected to a tensile load, a zone of inelastic deformation is induced at the tip of the crack. At the peak far-field tensile load, tensile stresses develop at the crack tip whose magnitude decays with distance according to the strength of the crack-tip singularity. If the far-field load is now released, the elastically deformed material outside the crack-tip plastic zone or damage zone exerts a 'clamping effect' on the crack tip provided that permanent deformation occurs at the crack tip (for example, due to dislocation plasticity, microcracking, phase transformation, creep cavitation, interfacial frictional sliding, crazing, shear banding, etc.). As a consequence, residual compressive stresses evolve at the crack tip upon unloading.

If an elastic-perfectly plastic solid is subjected to far-field cyclic tensile loads, the size of the plane stress cyclic plastic zone, r_c, directly ahead of the crack tip is[1]

$$r_c \approx \frac{1}{4\pi}\frac{\Delta K^2}{\sigma_{y,c}^2} \tag{1}$$

Here $\Delta K = K_{max} - K_{min}$ is the applied stress-intensity factor range, K_{max} and K_{min} are the maximum and minimum values, respectively, of the stress intensity factor during the fatigue cycle. The peak monotonic plastic zone size is

$$r_p = \frac{1}{\pi}\frac{K_{max}^2}{\sigma_y^2} \tag{2}$$

For zero–tension–zero far-field cyclic loading, the cyclic plastic zone for the elastic-perfectly plastic solid is one-quarter the size of the monotonic plastic zone. It is implicitly assumed that the monotonic and cyclic yield strengths, σ_y and $\sigma_{y,c}$, respectively, are the same. For steady-state fatigue crack growth under plane stress, the size of the cyclic plastic zone has been estimated to be about one-tenth of the monotonic plastic zone, the basis of the Dugdale strip yield model[2]. The cyclic plastic or damage zone size for various materials, loading conditions and constitutive responses is summarized in *Table 1*.

Cyclic residual stress fields are not unique to elastic-perfectly plastic materials. This zone of reversed damage is the result of permanent strains that are retained in the near-tip region upon unloading. Such permanent damage mechanisms can be as diverse as martensitic transformations and dislocation plasticity in metals, microcracking and grain boundary sliding in ceramics, and shear localization and crazing in polymers. Within the cyclic damage zone, residual compressive stresses are generated upon unloading from far-field tensile stress and residual tensile stresses are created upon unloading from far-field compressive stress (provided that the crack faces do not fully close during the entire compression load cycle), see *Figure 1*.

The evolution of cyclic near-tip stress fields ahead of fatigue cracks is known to have a pronounced effect on the fracture response. For instance, residual tensile stresses are responsible for the inception and growth of mode I fatigue cracks in notched components under fully compressive far-field cyclic loading in metals[3–6], ceramics[7–9] and polymers[10–12]. A compressive overload

* To whom correspondence should be addressed

0032-3861/94/15/3221–09

Table 1 Predicted cyclic damage zones for zero–tension–zero cyclic loads

Material	Cyclic plastic zone size	Monotonic plastic zone size
Elastic-perfectly plastic solid		
Stationary crack (ref. 1)[a]	$r_c \approx \Delta K^2/(4\pi\sigma_{y,c}^2)$	$r_p = K_{max}^2/(\pi\sigma_y^2)$
Steadily growing crack (ref. 2)[a]	$r_c \approx \Delta K^2/(10\pi\sigma_{y,c}^2)$	$r_p = K_{max}^2/(\pi\sigma_y^2)$
Microcracking solid (ref. 5)[b]	Up to 9ρ	–
Interface fatigue crack[c]	$r_c \approx r_p/5$	–
Crazing polymer	$r_c \approx \pi\Delta K^2/(32\sigma_{y,c}^2)$[d]	$s = \pi K_{max}^2/(8\sigma_y^2)$

[a] Plane stress
[b] ρ = crack-tip radius; analysis conducted for plane strain, stress-induced microcracking in alumina
[c] For a stationary fatigue crack along the interface between a metal and a ceramic; finite element simulations for plane strain (after Woeltjen, C., Shih, C. F. and Suresh, S. *Acta Metall. Mater.* 1993, **41**, 2317)
[d] Experimentally determined, this study. s refers to the craze zone size

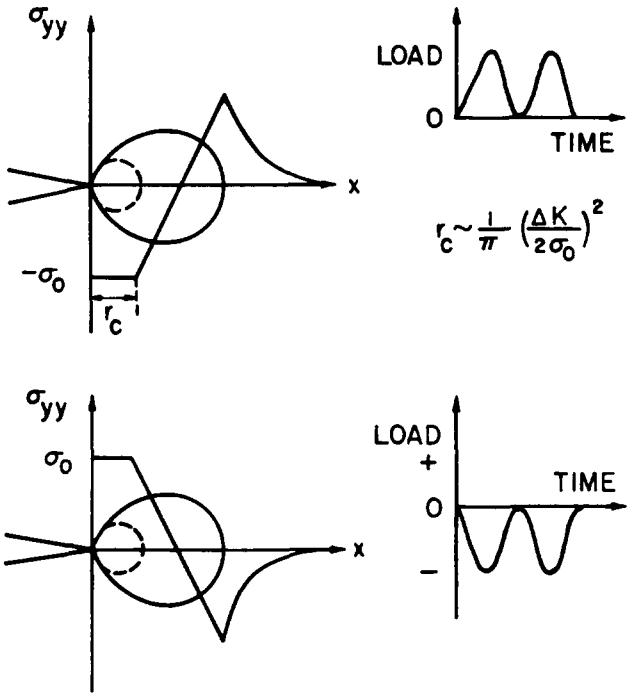

Figure 1 Schematic representation of cyclic plastic zones ahead of non-closing fatigue flaws in elastic-perfectly plastic solids partially unloaded during (a) cyclic tension; (b) cyclic compression

can, in fact, be detrimental to a component as the residual tensile stresses induced at the crack tip can result in the exacerbation of fatigue fracture. Near-tip residual compressive stresses can also have a significant effect on the fatigue crack growth behaviour under cyclic tension loading. If a fatigue crack is subjected to a tensile overload, the residual compressive stresses induced at the crack tip upon unloading from far-field tension can persist for tens or hundreds of thousands of subsequent cycles (of smaller peak stress value). This residual compressive zone is considered to be one of the critical factors governing the retardation of post-overload crack growth in metals and non-metals[13,14].

In order to understand the conditions responsible for fracture and damage ahead of fatigue cracks, it is necessary to make quantitative measurements of the components of cyclic near-tip stresses. Only a few studies, however, have provided quantitative information on the extent of cyclic damage and cyclic near-tip fields. In metallic materials, X-ray methods have been used to determine the average residual stresses ahead of fatigue cracks which are subjected to overloads[15] and neutron diffraction techniques have been used to measure normal residual stresses ahead of compression fatigue cracks[16]. These studies were performed at the completion of the fatigue test (and not *in situ*), and the underlying stress analyses did not determine all the different components of the stress field. Recently, the authors of the present paper have provided quantitative information about the evolution of cyclic damage zones in polymers subjected to fully compressive far-field loading using *in situ* laser interferometry and photoelasticity[17]. This study offered direct measurements of reversed damage zones, residual tensile stresses and their effect on fatigue crack propagation ahead of notches under fully compressive loading. To our knowledge, no such studies have hitherto been carried out in the cyclic tension of polymers.

In this paper, direct and *in situ* experimental measurements of cyclic stress fields ahead of tension fatigue cracks in a model amorphous solid (polycarbonate resin) are presented. Photoelasticity and laser interferometry experiments are conducted on compact tension specimens of the photoelastic resin to determine the residual stresses within the near-tip damage zone during the inception and propagation of the fatigue crack from the stress concentration. These analyses provide experimental validation of the existence of a zone of residual compressive stresses within the cyclic damage zone ahead of the tension fatigue crack. Furthermore, transmission electron microscopy (TEM) analyses of the crack-tip region in polycarbonate and rubber-modified polystyrene have also been conducted to determine the micromechanisms of damage ahead of the fatigue crack.

EXPERIMENTAL

Materials

The experimental work reported in this paper focuses on a polycarbonate (PC) resin and a rubber-modified, high-impact polystyrene (HIPS). Polycarbonate was used, because of its amenability to photoelastic analyses, as a model material for quantifying the cyclic stress fields. The rubber-modified polystyrene was chosen for its susceptibility to crazing and its amenability to detailed transmission electron microscopic analyses. (In our earlier experimental work on compression fatigue, a direct link was established between the evolution of cyclic near-tip fields, as quantified in the photoelastic resin, and the evolution of cyclic damage by crazing, as observed in the TEM in specimens of HIPS.)

The PC polymer was obtained in plate form under the commercial name Lexan, a product of GE, Schenectady, NY. It has a weight-average molecular weight of 35 000. PC has the following mechanical properties at room temperature: tensile yield strength = 30 MPa, ultimate tensile strength = 32 MPa and tensile modulus = 2.95 GPa. PC has the following stress-optical properties: fringe stress coefficient, $f = 13.8\ \mathrm{kN\,m^{-1}}$, and stress optic material constants, $A = -93.3 \times 10^{-12}\ \mathrm{m^2\,N^{-1}}$ and $B = -100 \times 10^{-12}\ \mathrm{m^2\,N^{-1}}$. ($f$, A and B are defined in the following sections.)

The rubber-modified polystyrene polymer was obtained from Dow Chemical Co., Midland, MI. The HIPS is amorphous; its weight-average molecular weight, M_w, is 240 000 and its number-average molecular weight, M_n, is 86 000 (i.e. a polydispersity of 2.8). The polystyrene is modified with 7.5 wt% butadiene rubber in the form of gel particles which have an average diameter of 1–2 μm. The HIPS has the following mechanical properties at room temperature: tensile yield strength = 18 MPa, ultimate tensile strength = 16.6 MPa and tensile modulus = 1.65 GPa.

Mechanical tests

All tension fatigue experiments were performed using compact tension specimens. The compact specimen dimensions are: length $L = 19$ mm, width measured from the centre of holes $W = 15$ mm, height $2H = 19$ mm, notch length $a_0 = 5.33$ mm, notch-root radius $\rho = 0.5$ mm, and notch-tip angle $\theta = 60°$. This notch geometry is the same as that employed in the cyclic compression test specimens. The thicknesses of the PC and HIPS specimens are $T = 2.54$ mm and $T = 3.17$ mm, respectively. All experiments were conducted using a servohydraulic closed loop testing machine in the laboratory air environment at a temperature of about 23°C and relative humidity of about 60%. The loading frequency ν was chosen to be 5 Hz, to avoid hysteretic heating effects, with a sinusoidal waveform and a load ratio $R = 0.1$. The load ratio, R, is defined as the ratio of minimum load to the maximum load of the fatigue cycle, $R = \sigma_{min}/\sigma_{max}$. The fatigue crack was monitored *in situ* using a Questar long-range microscope and video image processor; full details are given elsewhere[17].

Photoelasticity

Photoelastic stress analyses were performed on compact specimens of the resin subjected to cyclic tension loads. Photoelastic resins are isotropic in the unstressed state and become optically anisotropic when stressed. When a polarized beam of light passes through a two-dimensional photoelastic material stressed in its plane, the light is split into two perpendicular components which coincide with the principal stress directions. The velocities of these light components are directly proportional to the magnitudes of the principal stresses. This results in a relative retardation between the two components as they emerge from the model, and if white light is used, as it is in these experiments, a series of brilliantly coloured fringes, termed isochromatics, develop. The isochromatics are lines of constant colour due to the varying values of relative retardation at different points of the specimen and are a direct measure of the principal stress difference. The principal stress

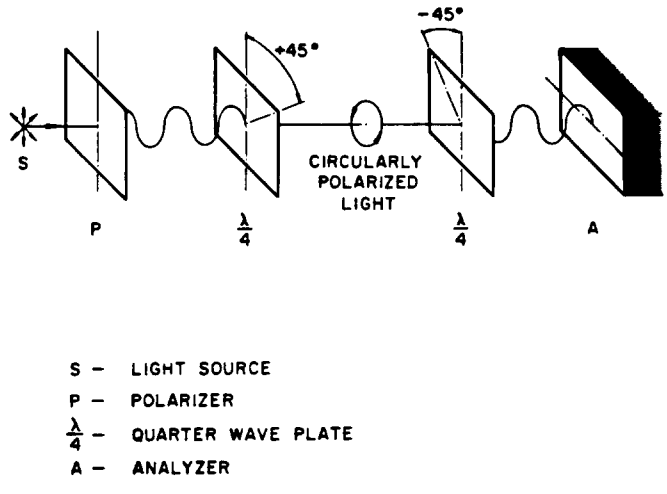

Figure 2 Schematic representation of the crossed circular polariscope used in photoelastic experiments

difference is found using the stress-optic law:

$$(\sigma_1 - \sigma_2) = \frac{nf}{T} \tag{3}$$

where the fringe order n is the number of wavelengths of interference, f is the fringe stress coefficient and T is the specimen thickness.

If plane polarized light is passed through the stressed photoelastic model, the resulting fringe pattern is an overlay of isochromatics and isoclinics. The latter are lines of equal angle and are the loci of points along which the principal stresses have parallel directions to the optic axes of the polarizer and analyser. These points result in extinction regardless of the magnitude of $(\sigma_1 - \sigma_2)$. If, instead, the incident light is polarized such that its plane of polarization rotates with time at a constant angular velocity ω (i.e. if the incident beam is circularly polarized), only the isochromatic pattern appears. *Figure 2* is a schematic of the circular polariscope which is used to obtain the isochromatic fringe patterns. The isoclinics are obtained through the plane polariscope, this conversion is done by simply removing the $\lambda/4$ plates. The isoclinics are determined by rotating the crossed polars in the plane polariscope with a white light source and are usually sketched or traced at 10–15° intervals.

The isochromatics give lines of constant $(\sigma_1 - \sigma_2)$ as determined from equation (3), and the isoclinics provide the loci of points along which the principal stress directions are parallel. If θ is the angle that the maximum principal stress makes with the x-axis, the shear stress at a given point on the x–y plane is given by

$$\tau_{xy} = \frac{(\sigma_1 - \sigma_2)}{2} \sin 2\theta \tag{4}$$

Laser interferometry

In order to measure the loci of equal sums of principal stresses, $(\sigma_1 + \sigma_2)$, a Mach–Zehnder laser interferometer technique was employed. A schematic of the laser interferometer is shown in *Figure 3*. The monochromatic light source was a helium–neon laser. A model with an initially flat surface subjected to a two-dimensional stress (plane stress) state loses its optical flatness upon the application of the load. Each interference fringe pattern represents a line of constant thickness (isopachic curve).

The laser interferometer splits its beam into two optical paths (with one of the paths passing through the crack-tip region of the transparent photoelastic material) which are then recombined creating an interference pattern[18]. The principal stress sum is given by the expression

$$(\sigma_1+\sigma_2)=\frac{2N_p\lambda}{T(A+B)} \quad (5)$$

where N_p is the isopachic fringe order, and A and B are stress-optic constants.

Stress analysis

The stress patterns and fringes from both photoelasticity and laser interferometry were monitored *in situ* during the fatigue test at different stages of loading and unloading (and as a function of the number of fatigue cycles and hence, crack length) using a colour video camera and a video image processor. In the photoelasticity measurements, the circular polariscope was converted into a plane polariscope by removing the $\lambda/4$ plates, and the isoclinic pattern, overlaid on the isochromatic fringes, was obtained by rotating the crossed polars at 15° intervals. The isoclinics were then separated from a knowledge of the base isochromatic patterns. Using the isochromatics, isoclinics and isopachics (from laser interferometry), the principal stresses were individually identified assuming plane stress deformation, and the cyclic stress fields surrounding the notch tip and fatigue crack tip were determined explicitly. Although a two-dimensional plane stress model was used in the present work, the possibility of any through-thickness variations in stresses is not expected to have any influence on the overall conclusions of this study. (The 'frozen stress techniques'[19] involving sectioning through the thickness of the specimen are not particularly applicable for the present *in situ* experiments.) Also, as shown later, the one-to-one correspondence between the experimentally measured cyclic damage zone size and the predicted values, as well as results found in previous work[17], strongly support the validity of the present experimental procedures and the interpretation of data.

TEM of crack-tip damage

With the objective of establishing the micromechanisms of crack-tip damage, detailed TEM was performed in the immediate vicinity of the fatigue crack tip. As noted earlier, in addition to the PC, the HIPS was chosen for this purpose because of its well known susceptibility to crazing.

After the crack had propagated some distance under cyclic tension loads, the specimens were sectioned for TEM observations. A small rectangular section, inclusive of the fatigue crack tip and the crack-tip damage zone, was removed with a jeweller's saw. This section was embedded in an impregnating resin (spurr) and cured for 24 h. The embedded specimen was then microtomed into ultrathin sections, which were cut parallel to the front face of the specimen (in order to study the damaged region in front of the fatigue crack tip) using a diamond knife and a Reichler™ microtome. These ultrathin sections were then placed onto 3 mm diameter copper support grids and the HIPS specimens were stained with osmium vapour. The osmium tetroxide reacts with the double carbon–carbon bonds in the unsaturated butadiene phases and enhances TEM contrast by increasing electron scattering of the heavy metal in the rubber particles.

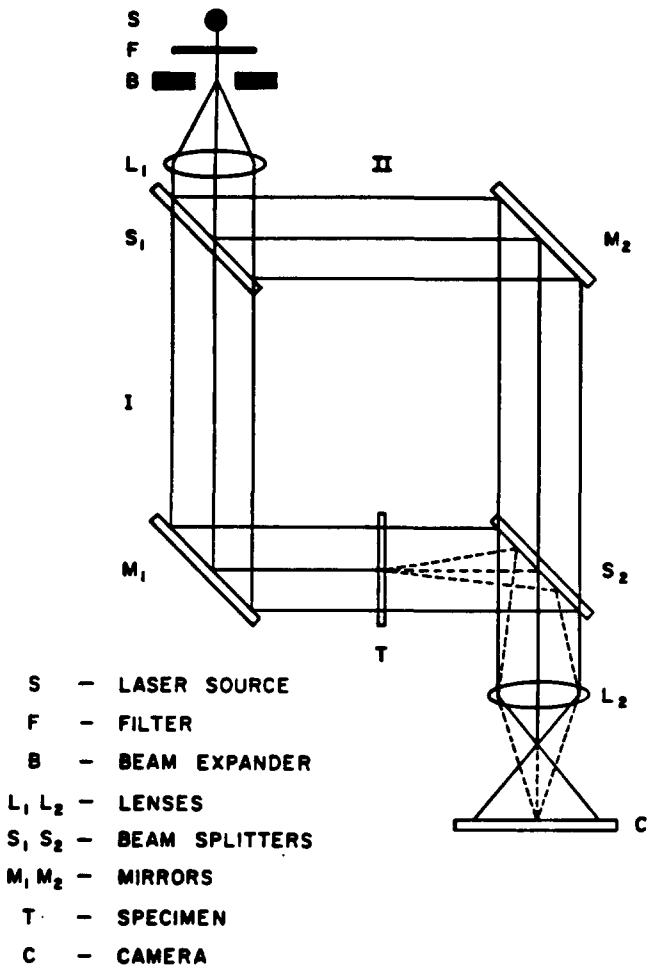

Figure 3 Schematic representation of Mach–Zender laser interferometer

To ensure that TEM observations were a proper indication of the damage mechanisms and not a consequence of specimen preparation, an identical TEM sample preparation was used on the as-received (untested) materials. Such comparisons revealed that the TEM observations reported in this paper are not artifacts of the specimen preparation procedure; this was also verified in our previous study[17]. All the TEM observations reported here were made on a Phillips EM 420T electron microscope operating at a voltage of 120 kV.

RESULTS

Cyclic near-tip stress measurements

Figures 4a, b are optical micrographs of the isochromatic fringe patterns of the notch-tip region of the compact tension specimen of the photoelastic resin during different stages of unloading in the very first tension fatigue cycle. These micrographs were taken for $K=0.57$ MPa $m^{1/2}$ and $K=0.06$ MPa $m^{1/2}$, respectively. A knowledge of the fringe order obtained from these micrographs, in conjunction with equation (3), enables the determination of contours of constant principal stress difference $(\sigma_1-\sigma_2)$ in the near-tip region.

Figures 4c, d show the corresponding isopachic fringe patterns ahead of the crack, obtained with the

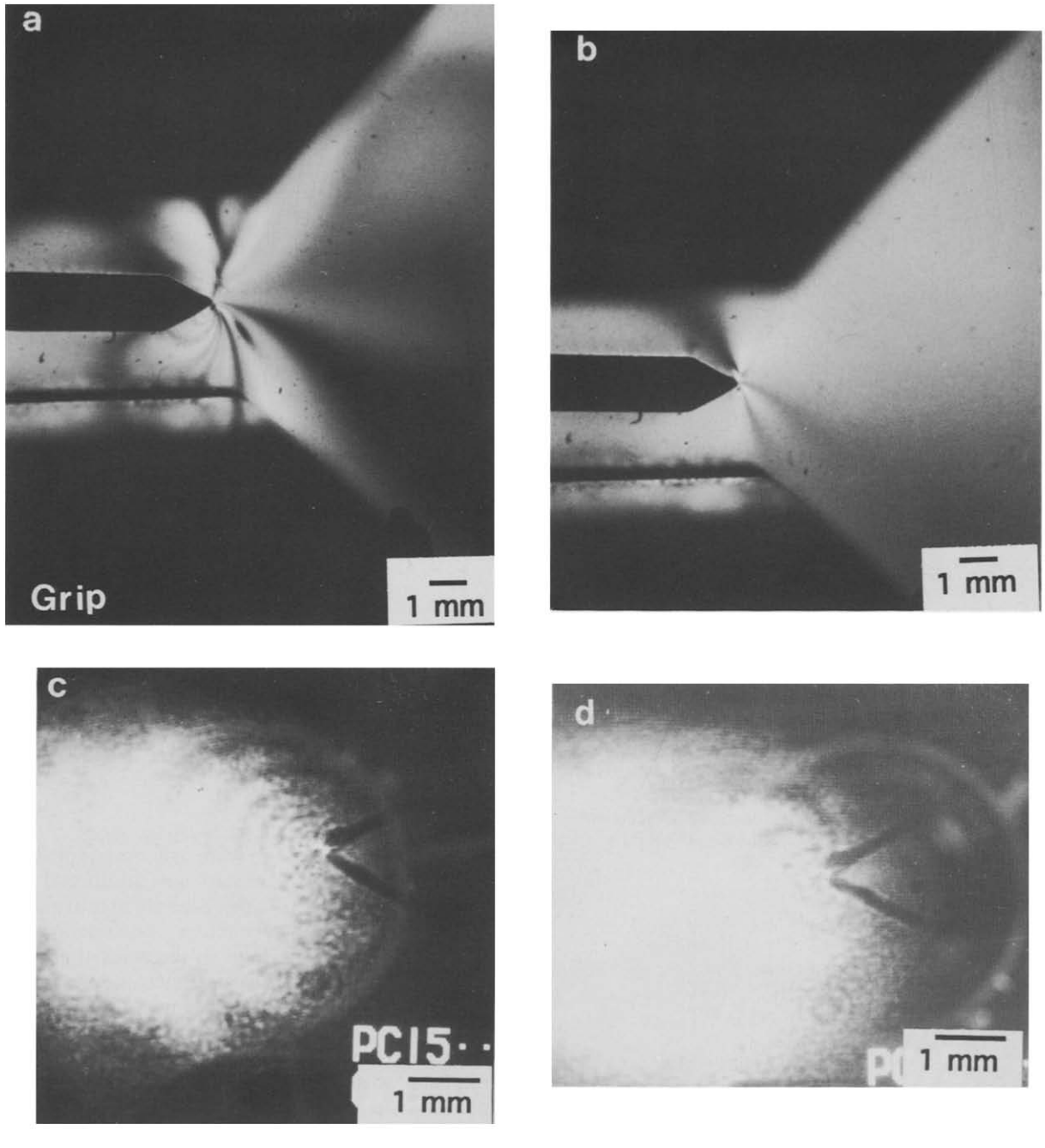

Figure 4 Micrographs of the isochromatic patterns as the specimen is unloaded in the first fatigue cycle to (a) $K=0.57\ \text{MPa m}^{1/2}$ and (b) $K=0.06\ \text{MPa m}^{1/2}$; corresponding optical micrographs of the isopachic patterns at (c) $K=0.57\ \text{MPa m}^{1/2}$ and (d) $K=0.06\ \text{MPa m}^{1/2}$

aid of the Mach–Zehnder laser interferometer, at $K=0.57\ \text{MPa m}^{1/2}$ and $K=0.06\ \text{MPa m}^{1/2}$, respectively. The isopachic fringes, in conjunction with equation (5), provide the principal stress sums, $(\sigma_1+\sigma_2)$. The overlay of the isochromatic and isopachic fringe patterns during the different stages of unloading in the first tension cycle is illustrated in *Figures 5a, b*. By combining the stress patterns, the principal stresses σ_1 and σ_2 can be individually identified wherever the isopachics and the isochromatics intersect.

The information contained in *Figure 5* was then combined with the isoclinics (taken at $K=0.06\ \text{MPa m}^{1/2}$), shown in *Figure 6*, to determine the angle θ, used in equation (4). With this information, the normal stresses σ_{xx} and σ_{yy} and the shear stress τ_{xy} (in the plane stress model) can be individually identified using the following relationships:

$$\sigma_1=\frac{(\sigma_{xx}+\sigma_{yy})}{2}+\left\{\tau_{xy}^2+\frac{(\sigma_{xx}-\sigma_{yy})^2}{4}\right\}^{1/2} \tag{6a}$$

$$\sigma_2=\frac{(\sigma_{xx}+\sigma_{yy})}{2}-\left\{\tau_{xy}^2+\frac{(\sigma_{xx}-\sigma_{yy})^2}{4}\right\}^{1/2} \tag{6b}$$

Of particular interest to mode I fatigue crack growth is the σ_{yy} component of stress acting on the plane of the crack. Values of σ_{yy} were determined for a multitude of geometric points surrounding the notch tip. *Figures 7a, b* show the contours of constant σ_{yy} so computed around the notch tip during the first fatigue cycle at $K=0.57\ \text{MPa m}^{1/2}$ and $K=0.06\ \text{MPa m}^{1/2}$, respectively. *Figure 7a* demonstrates that residual compressive stresses of $-3.8\ \text{MPa}$ over 0.5 mm are

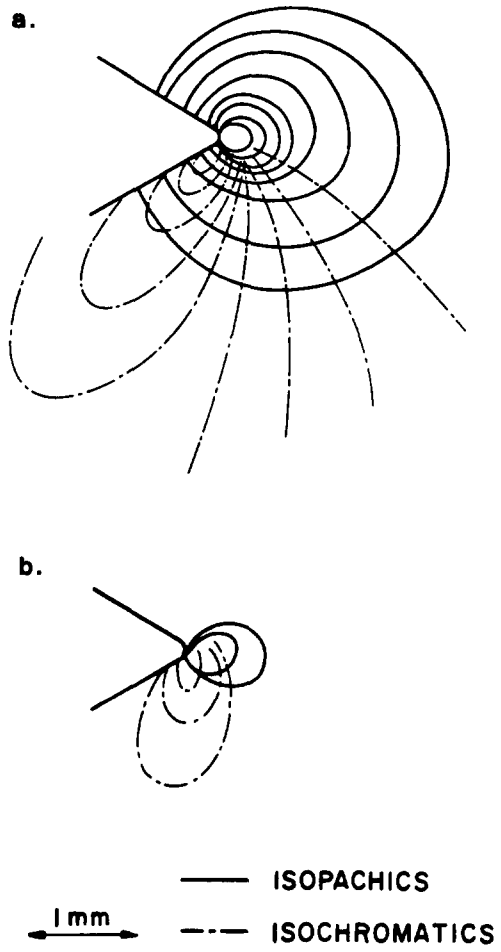

Figure 5 Overlay of the isochromatic and isopachic stress patterns as the specimen is unloaded in the first cycle to (a) $K=0.57$ MPa m$^{1/2}$ and (b) $K=0.06$ MPa m$^{1/2}$

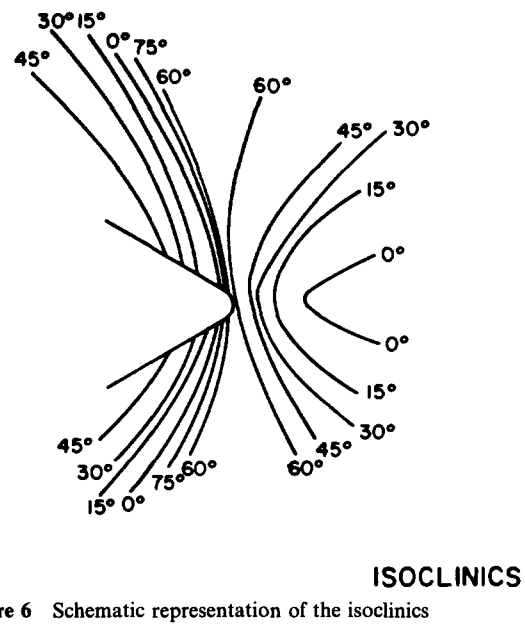

Figure 6 Schematic representation of the isoclinics

generated as the specimen is unloaded from far-field tension. As the specimen is unloaded further to $K=0.06$ MPa m$^{1/2}$ (*Figure 7b*), the magnitude of residual compressive stresses increases to -7.2 MPa over 0.3 mm and the distance of residual compression extends over 0.5 mm.

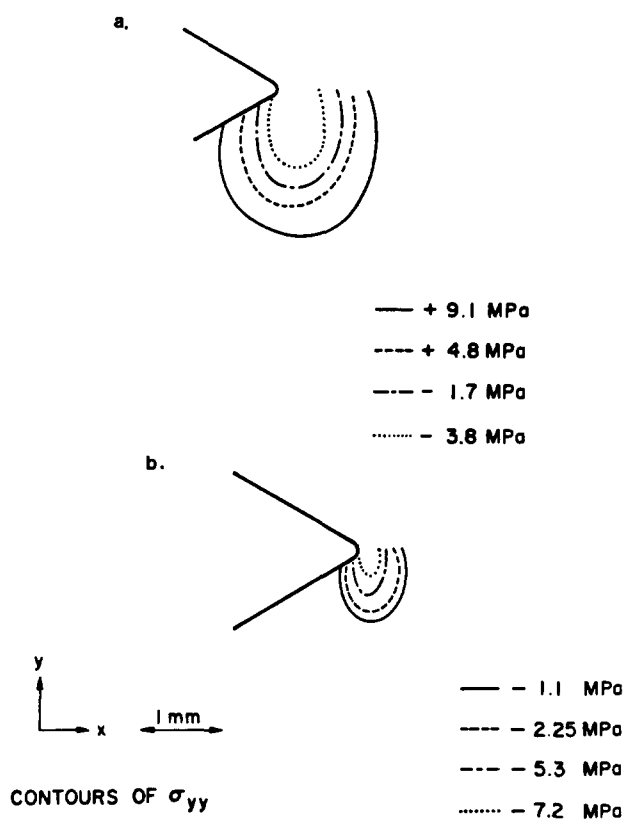

Figure 7 Contours of constant σ_{yy} at the notch tip as the specimen is unloaded in the first fatigue cycle to (a) $K=0.57$ MPa m$^{1/2}$ and (b) $K=0.06$ MPa m$^{1/2}$

Cyclic near-tip stresses were also determined after the fatigue crack had advanced an additional 3.33 mm ($\Delta K=0.98$ MPa m$^{1/2}$). *Figures 8a, b* are optical micrographs (obtained through a circular polariscope) of the isochromatic fringe patterns in the crack-tip region after 85 000 tension fatigue cycles. These micrographs were taken at $K=1.09$ MPa m$^{1/2}$ and $K=0.11$ MPa m$^{1/2}$, respectively. *Figures 8c, d* show the corresponding isopachic fringe patterns ahead of the fatigue crack, obtained with the aid of the Mach–Zehnder laser interferometer. The overlay of the isochromatic and isopachic fringe patterns during the different stages of unloading after 85 000 tension cycles is illustrated in *Figures 9a, b*.

Figures 10a, b show the contours of constant σ_{yy} around the crack tip after 85 000 fatigue cycles at $K=1.09$ MPa m$^{1/2}$ and $K=0.11$ MPa m$^{1/2}$, respectively. *Figure 10a* demonstrates that residual compressive stresses of -6.3 MPa over 0.5 mm are generated as the specimen is unloaded from far-field tension. As the specimen is unloaded to $K=0.11$ MPa m$^{1/2}$ (*Figure 10b*), the magnitude of residual compressive stresses increases to -9.4 MPa over 0.35 mm and the distance of residual compression extends over 1.1 mm.

TEM observations

Figure 11a is a transmission electron micrograph of the microscopic damage within the cyclic damage zone in PC. The primary deformation mechanism here is the breakdown of the craze fibrils, possibly due to the imposition of the residual compressive stresses. *Figure 11b* is a transmission electron micrograph taken

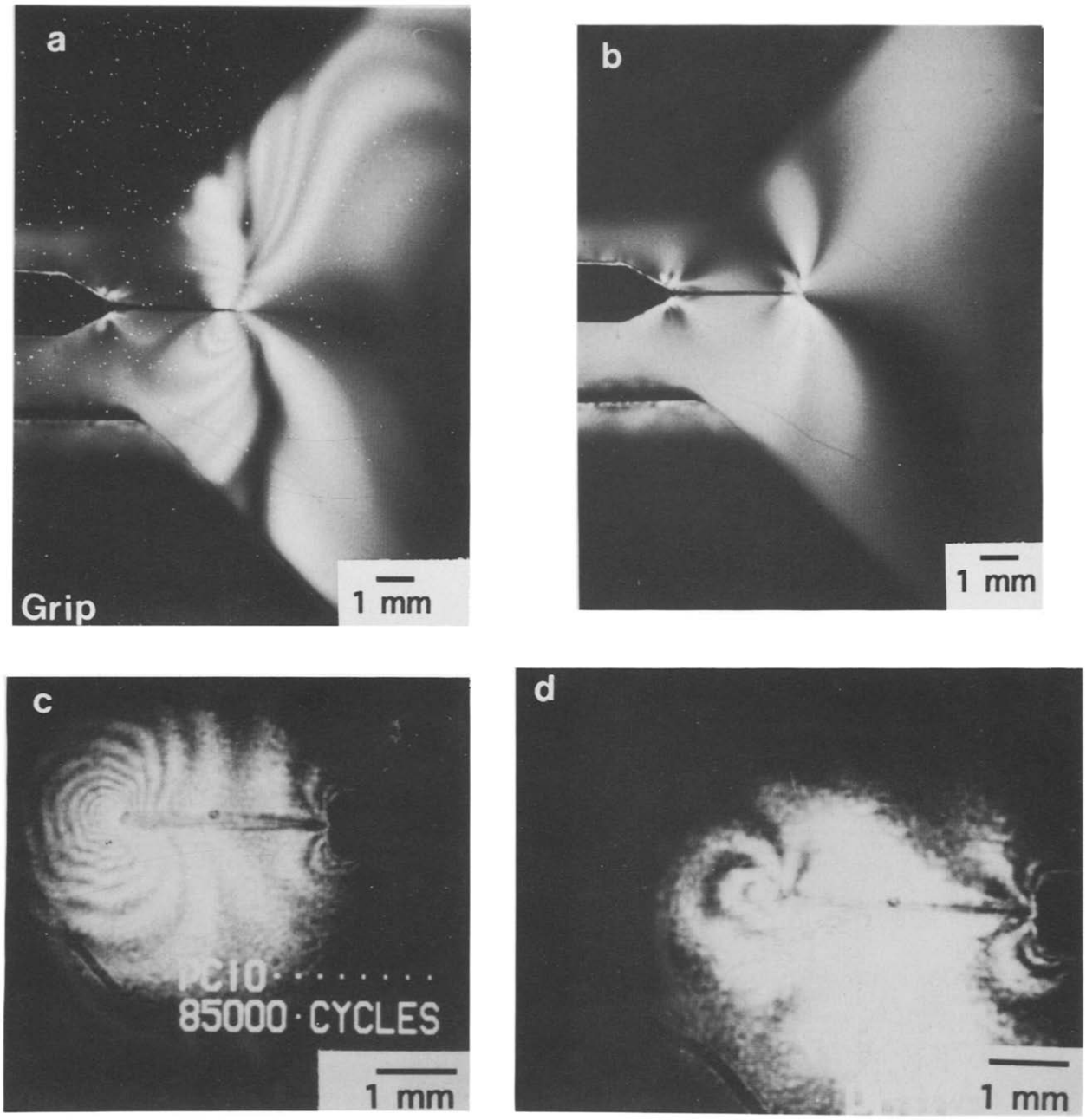

Figure 8 Optical micrographs of the isochromatic patterns as the specimen is unloaded after 85000 fatigue cycles to (a) $K = 1.09$ MPa m$^{1/2}$ and (b) $K = 0.11$ MPa m$^{1/2}$; corresponding optical micrographs of the isopachic patterns at (c) $K = 1.09$ MPa m$^{1/2}$ and (d) $K = 0.11$ MPa m$^{1/2}$

in front of the cyclic damage zone where stresses are tensile in nature; the primary deformation mechanism is craze formation and the craze is of the fibrillar structure with fibrils typically 30 nm in diameter.

Figure 12a is a transmission electron micrograph of microscopic damage within the cyclic damage zone ahead of the tension fatigue crack in the HIPS. This micrograph indicates that the primary deformation mechanism directly ahead of the fatigue crack tip is craze breakdown. The fibrils of the crazes have failed and have left behind a region of microcracks or voids. *Figure 12b* is a transmission electron micrograph of microscopic damage in front of the cyclic damage zone. Here the primary deformation mechanism is crazing, the crazes are identified as fine bands with fibrillar structure, where the fibrils are typically 20 nm in diameter.

DISCUSSION

The quantitative stress measurements provide a clear and unambiguous verification of the existence of a zone of residual compressive stresses within the near-tip damage zone. The residual compressive stresses evolve during unloading from a far-field tensile stress. Furthermore, the total distance of residual compression measured using experimental stress analysis is consistent with the cyclic damage zone size predicted from fracture mechanics, i.e. one-quarter the size of the monotonic plastic zone. The craze zone size is predicted using the Dugdale strip yield model (see ref. 5 for a critical review):

$$s = \frac{\pi}{8}\frac{K_{max}^2}{\sigma_c^2} \tag{7}$$

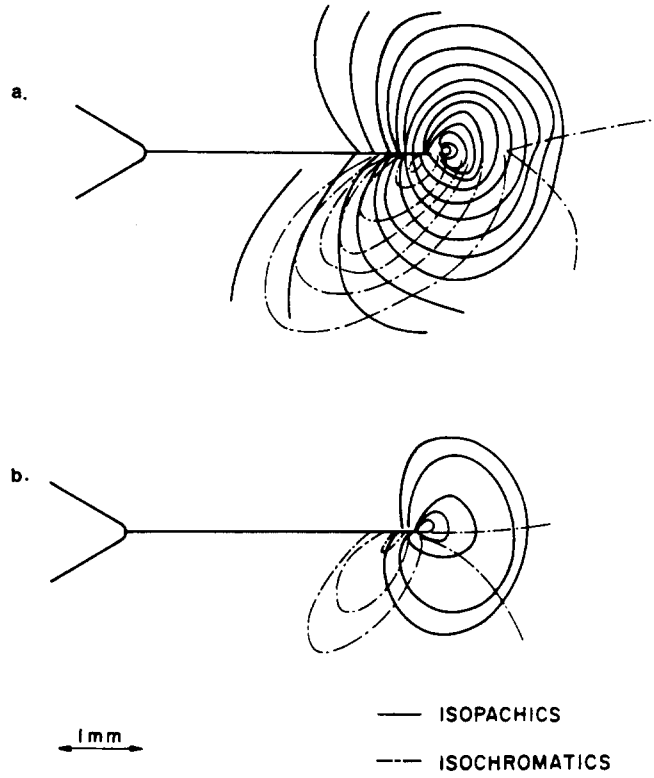

Figure 9 Overlay of the isochromatic and isopachic stress patterns as the specimen is unloaded after 85 000 fatigue cycles to (a) $K = 1.09$ MPa m$^{1/2}$ and (b) $K = 0.11$ MPa m$^{1/2}$

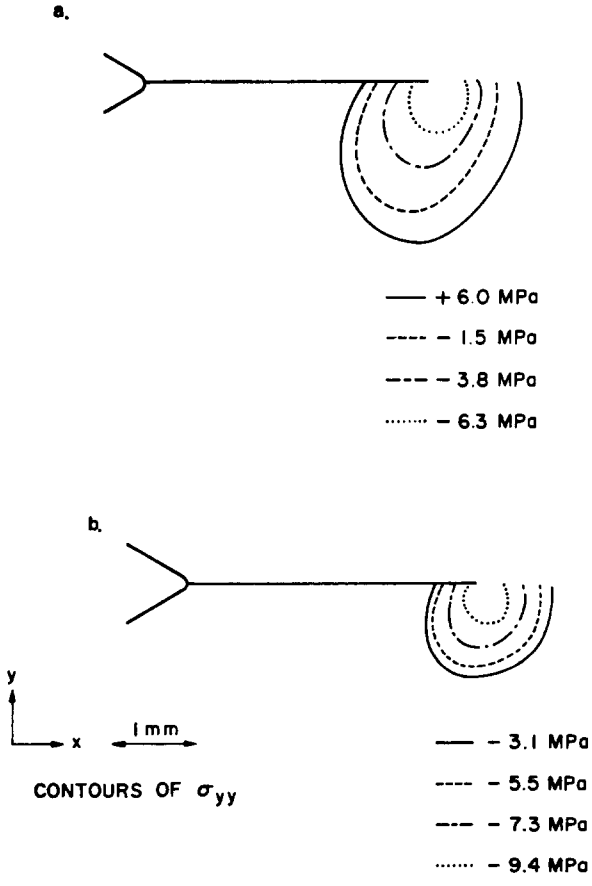

Figure 10 Contours of constant σ_{yy} at the notch tip as the specimen is unloaded after 85 000 fatigue cycles to (a) $K = 1.09$ MPa m$^{1/2}$ and (b) $K = 0.11$ MPa m$^{1/2}$

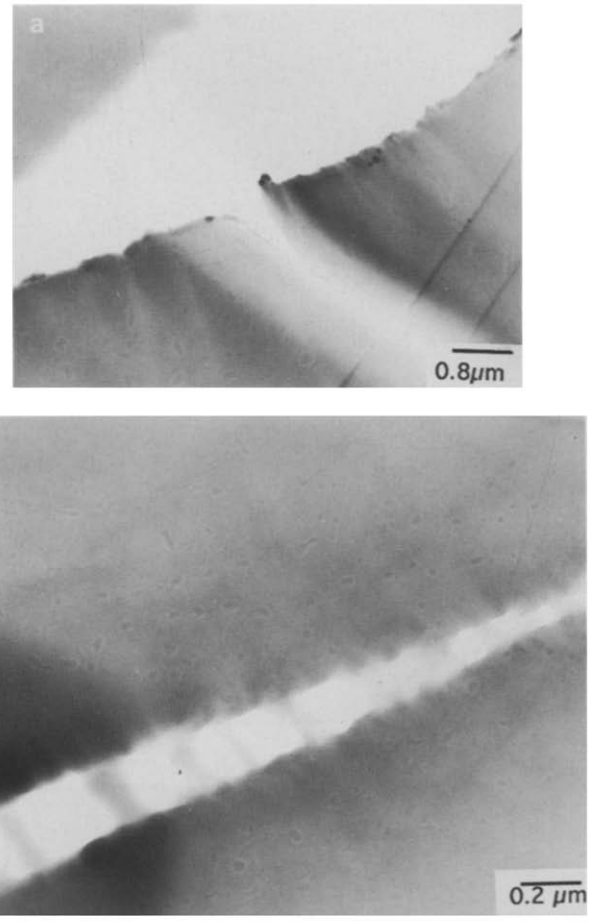

Figure 11 TEM micrographs of PC (a) directly in front of fatigue crack tip demonstrating fibril breakdown; and (b) the region further out in front of the fatigue crack, where there is evidence of crazing with fibrils still intact

Table 2 Correlation of experimentally measured and predicted cyclic damage zone size, r_c

Crack length (mm)	Experimental r_c (mm)	Predicted r_c (mm)
0.2 (1st cycle)	0.48	0.38
3.3 (85 000 cycles)	1.1	0.94

where s is the craze or plastic zone size and σ_c is the crazing stress of the polymer. In the first fatigue cycle, ($\Delta K = 0.62$ MPa m$^{1/2}$), the predicted cycle damage zone size is 0.38 mm whereas the experimentally measured value was 0.48 mm. After 85 000 cycles, ($\Delta K = 0.98$ MPa m$^{1/2}$), the predicted cycle damage zone size is 0.94 mm and the experimentally measured value was 1.1 mm (see *Table 2*).

The primary focus of this study has been cyclic fields ahead of fatigue cracks in polymers subjected to constant amplitude cyclic stresses; however, these results also have strong implications for variable-amplitude fatigue as well as for other materials. For example, if a ductile material is subjected to a tensile overload, greater levels of residual compressive stresses are created at the crack tip upon unloading[20]. These residual compressive stresses play a critical role in determining the extent of crack growth retardation which is generally seen after the application of the overload. In addition, the application of the tensile

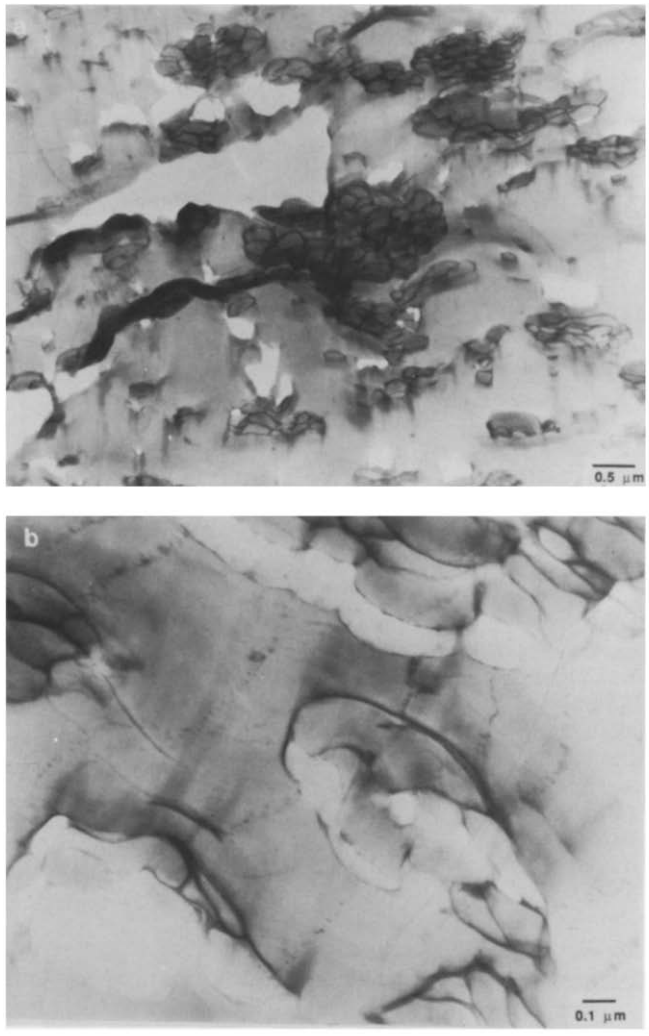

Figure 12 TEM micrographs of HIPS in (a) the region directly in front of the fatigue crack, demonstrating evidence of crazing where fibrils have broken down; (b) the region further out in front of the fatigue crack, where there is evidence of crazing with fibrils still intact

overload can result in a blunted crack tip which could then serve as a notch. If this blunted crack tip were followed by a compressive overload, residual tensile stresses would be created upon unloading which can partially or fully offset the previously created residual compressive stresses at the crack tip. Such effects can significantly affect the crack growth behaviour and total life of a component during variable amplitude fatigue.

CONCLUSIONS

- Experimental results are presented which document *in situ* measurements of the evolution of cyclic stress fields ahead of a fatigue crack subjected to cyclic tension loading.
- Photoelasticity and laser interferometry studies of a model resin were employed to demonstrate directly that compressive near-tip residual stresses evolve ahead of notches and sharp fatigue cracks subjected to far-field cyclic tension loading.
- The generation of residual compressive stresses is most effective in the final stages of unloading, especially when the peak stress of the fatigue cycle approaches values close to zero.
- Transmission electron microscopy of the crack-tip region in high-impact polystyrene and polycarbonate demonstrates that crazing is the mechanism of deformation under cyclic tension loads. Crazing leads to permanent strains at the crack tip, which upon load reversals create a cyclic damage zone. The tension fatigue crack advances due to the breakdown of fibrils in the craze zone.

ACKNOWLEDGEMENTS

This work was supported by the Office of Naval Research under Grant N00014-89-J-3099 to Brown University and under N00014-93-1-1399 to MIT. The authors thank Drs G. Yoder and A. K. Vasudevan for their support of the work and for helpful discussions.

REFERENCES

1 Rice, J. R. ASTM STP 415, 1967, p. 247
2 Budianski, B. and Hutchinson, J. W. *J. Appl. Mech.* 1978, **45**, 267
3 Hubbard, R. P. *J. Basic Eng.* 1969, **91**, 625
4 Reid, C. N., Williams, K. and Hermann, R. *Fatigue Fract. Eng. Mater. Struct.* 1979, **1**, 267
5 Suresh, S. 'Fatigue of Materials', Cambridge University Press, Cambridge, 1991
6 Holm, D. K., Blom, A. F. and Suresh, S. *Eng. Fract. Mech.* 1986, **23**, 1097
7 Ewart, L. and Suresh, S. *J. Mater. Sci.* 1987, **22**, 1173
8 Suresh, S. and Brockenbrough, J. R. *Acta Metall.* 1988, **36**, 1455
9 James, M. N., Tait, R. B. and Mech, D. G. *Fatigue Fract. Eng. Mater. Struct.* 1991, **14**, 227
10 Suresh, S. and Pruitt, L. in 'Deformation, Yield and Fracture of Polymers', Proc. 8th International Conference, Churchill College, Cambridge University, April 1991, The Plastics and Rubber Institute, London, 1991, p. 32-1
11 Pruitt, L., Hermann, R. and Suresh, S. *J. Mater. Sci.* 1992, **27**, 1608
12 Pruitt, L. and Suresh, S. *J. Mater. Sci. Lett.* 1992, **11**, 1356
13 Wheeler, O. E. *J. Basic Eng.* 1972, **94**, 181
14 Willenborg, J., Engle, R. M. and Wood, H. 'Tech. Report TFR 71-701', North American Rockwel, Los Angeles, CA, 1971
15 Allison, J. E. ASTM STP 677, 1979, p. 550
16 Reid, C. N., Moffatt, J. and Hermann, R. *Scripta. Met.* 1988, **22**, 1743
17 Pruitt, L. and Suresh, S. *Phil. Mag. A* 1993, **67**, 1219
18 Nisida, M. and Saito, H. *Exp. Mech.* 1964, **4**, 366
19 Frocht, M. M. and Leven, M. M. *J. Appl. Phys.* 1942, **13**, 308
20 Banasiak, H. *J. Appl. Polym. Sci.* 1977, **21**, 1279